INSERT CREATIVE NAME HERE

Author's name

Bachelorarbeit in Physik
angefertigt im Argelander-Institut für Astronomie

vorgelegt der
Mathematisch-Naturwissenschaftlichen Fakultät
der
Rheinischen Friedrich-Wilhelms-Universität
Bonn

MMM 2024

Ich versichere, dass ich diese Arbeit selbstständig verfasst und keine anderen als die angegebenen Quellen und Hilfsmittel benutzt sowie die Zitate kenntlich gemacht habe.

Bonn,	. . . .	. . . .
	Datum	Unterschrift

1. Gutachter: Prof. Dr. John Smith
2. Gutachterin: Prof. Dr. Anne Jones

Acknowledgements

I would like to thank ...

You should probably use `\chapter*` for acknowledgements at the beginning of a thesis and `\chapter` for the end.

Contents

CHAPTER 1

Introduction

Testing Kolokythas et al., 2020. new line

CHAPTER 2

Theoretical Background

2.1 Clusters and groups of galaxies

Throughout the Universe, galaxies are not distributed homogeneously but are instead aggregated into massive cosmic structures known as galaxy groups or galaxy clusters. Galaxy clusters – the largest relaxed structures in the Universe – typically have masses exceeding $M \gtrsim 3\times10^{14} M_{\odot}$, whereas galaxy groups have masses around $M \sim 3 \times 10^{13} M_{\odot}$ (Schneider, 2006). Advancements in X-ray astronomy have demonstrated that these structures are significant sources of X-ray radiation (Cavaliere, Gurksy, and Tucker, 1971). This emission is well understood to originate from a hot intergalactic gas known as the intracluster medium (ICM), which is characterized by temperatures in the range of 10^7 to 10^8 K and constitutes the primary baryonic component of galaxy clusters (Schneider, 2006).

2.1.1 The Intracluster Medium (ICM)

Within the deep gravitational wells of galaxy clusters, the temperatures become sufficiently high to fully ionize lighter elements and partially ionize heavier elements, resulting in the formation of a plasma. This hot, diffuse, and optically thin plasma, known as the Intracluster Medium (ICM), emits significant amounts of X-ray radiation. X-ray analysis of the ICM have enabled a wide variety of cosmological studies, including large-scale structure formation in the Universe (Kravtsov and Borgani, 2012).

2.1.2 Emission Processes within the ICM

A key principle of electrodynamics is that accelerated charges radiate energy. This radiation is referred to as bremsstrahlung or "free-free" when a free charged particle, typically an electron, is accelerated by the electric field of other charges, usually ions. In the ICM, this process predominates at temperatures above $k_B T_e \gtrsim 2\,\mathrm{keV}$, where the total emissivity at solar metallicity scales approximately as

$$\epsilon_{\mathrm{ff}} \propto T_{\mathrm{e}}^{\frac{1}{2}} n_{\mathrm{e}},$$

with n_e and T_e as the electron number density and temperature, respectively. At lower temperatures ($k_B T \lesssim 2\,\mathrm{keV}$), line emission becomes significant, with the emissivity being roughly described by

$$\epsilon \propto T_e^{-0.6} n_e.$$

2.1.3 The galaxy group NGC1550

Insert cool stuff about cluster here

2.2 eROSITA

The extended ROentgen Survey with an Imaging Telescope Array (eROSITA) is a highly sensitive, wide-field X-ray telescope designed to capture deep and precise images across large areas of the sky. Mounted on the Spektrum-Roentgen-Gamma (SRG) observatory in a halo orbit around the second Lagrange Point, eROSITA operates within the 0.2 to 10.0 keV energy range. It is the first instrument to perform an all-sky imaging survey in the hard X-ray band (2.0 to 10.0 keV). In the soft X-ray band (0.5 to 2.0 keV), eROSITA boasts a sensitivity that is approximately 20 times greater than that of its predecessor, the ROSAT All-Sky Survey. eROSITA features seven identical mirror modules, known as Telescope Modules (TMs), each with 54 mirror shells in Wolter-I geometry and a 1.6-meter focal length. Five TMs (TM1, TM2, TM3, TM4, TM6) have aluminum on-chip optical light filters and are collectively referred to as TM8. The remaining two TMs (TM5, TM7), designed for low-energy spectroscopy, lack these filters and are referred to as TM9. (Predehl et al., 2021). Collectively, TM8 and TM9 are referred to as TM0.

2.3 Skybackground and contamination sources

For a thorough analysis of X-ray photons, it is essential to carefully consider both external background and internal instrumental contamination effects. The following section will provide a brief overview of the most important factors relevant to this analysis.

Cosmic X-ray Background (CXB): The Cosmic X-ray background comprises multiple sources, including diffuse, unabsorbed thermal emissions from the Local Hot Bubble, a plasma cavity surrounding the Sun, and absorbed thermal emissions from the Galactic halo (Galeazzi et al., 2006). Additionally, it includes discrete extragalactic sources, predominantly unresolved AGNs (Brandt and Hasinger, 2005). The diffuse component is more prominent in the lower energy band $\sim 1\,\mathrm{keV}$, while the extragalactic sources dominate at higher energies.

Non-X-ray Background (NXB): The non-X-ray background consists of two main components: highly variable soft protons flares from the solar corona and Earth's magnetosphere, which can be focused onto detectors, and energetic Galactic Cosmic Ray (GCR) primaries, which interact with the detector to produce secondary particles. While primary GCR events can be mostly discarded by onboard processing, the secondary particles deposit charge in the detector, making it challenging to distinguish them from true X-ray events. (Bulbul et al., 2020)

eROSITA light leak: Shortly after the launch of eROSITA, it was observed that CCDs lacking an on-chip filter (TM9) recorded a notably higher number of events. This was attributed to optical and ultraviolet light from the Sun entering the CCD through an unidentified gap in the detector shielding and was subsequently termed "light-leak" (Predehl et al., 2021).

Table 2.1: Fit Parameters

Region	1	2	3	4
West	$(2.38 \times 10^{-5}$	$(5.47 \times 10^{-1}$	$(1.11 \times 10^{2}$	$(1.01 \times 10^{-7}$
East	$(2.31 \times 10^{-5}$	$(4.96 \times 10^{-1}$	$(9.2 \times 10^{1}$	$(1.05 \times 10^{-7}$
North	$(1.69 \times 10^{-5}$	$(4.53 \times 10^{-1}$	$(8.1 \times 10^{1}$	$(8.08 \times 10^{-8}$
South	$(4.72 \times 10^{-5}$	$(4.99 \times 10^{-1}$	$(6.67 \times 10^{1}$	$(9.53 \times 10^{-8}$

CHAPTER 3

Data Reduction

In the following section, the underlying data shall be reduced and corrected for the various effects and contamination sources explained in Section 2.3. Data from eRASSX is utilized for for all TMs (1-7) using *eROSITA* pipeline processing version c010. The galaxy group NGC1550 is located in skytile 065087. In addition, the surrounding skytiles 062084, 062087, 062090, 065084, 065090, 068084, 068087, 068090 are used to encompass regions up to $\sim 3R_{200}$. The data reduction is performed with the software HEASoft version XXX and the extended Science Analysis Software System (eSASS 4DR1). Images were created using astropy.

3.1 Data preparation and filtering

For each skytile, the *eSASS* task `evtool` is employed with `pattern=15` to select single, double, triple, and quadruple event patterns, and `flag=0xc00fff30` to remove bad pixels and CCD corners. Subsequently, soft proton flares are identified and mitigated through the following process: using the `flaregti` task, light curves are generated with 20 s time bins within the energy range of 5 to 10 keV. A 3σ threshold is determined; time intervals exceeding this threshold indicate periods of elevated count rates likely caused by soft proton flares. The task `flaregti` is then rerun using this threshold to establish good-time-intervals (GTIs) excluding these flare periods, which are then applied using `evtool` with the `gti="FLAREGTI"` parameter.

3.2 Image Creation

To detect emission structures, one usually focuses on soft the X-ray band. In this analysis, we use the 0.2 to 2.3 keV energy band. Due to the light-leak in TM9 , however, the energy range is restrictated to 0.8 to 2.3 keV, while for TM8 it remains 0.2 to 2.3 keV.

CHAPTER 4

Data Analysis

4.1 Image Visual Inspection

4.2 Surface Brightness Analysis

To more precisely quantify possible asymmetries in the X-ray emission of NGC 1550, a surface brightness analysis is perfomed. These asymmetries can often signal recent dynamic events, such as galaxy mergers.

4.2.1 Azimuthal surface brightness

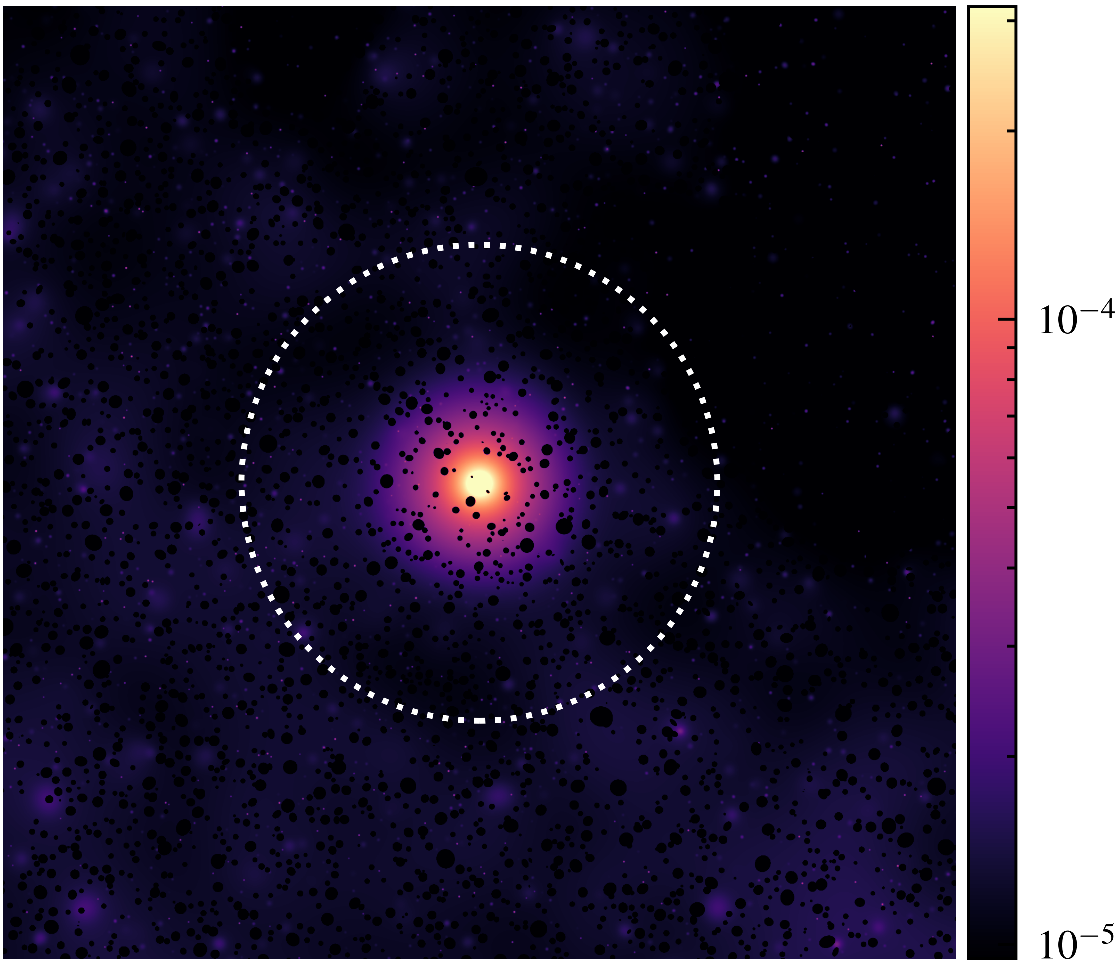

Figure 4.1: My image

Bibliography

Brandt, W. and G. Hasinger (2005), *Deep Extragalactic X-ray Surveys*, Annual Review of Astronomy and Astrophysics **43** 827, First published online as a Review in Advance on June 14, 2005 (cit. on p. 3).

Bulbul, E. et al. (2020), *Characterization of the Particle-induced Background of XMM-Newton EPIC-pn: Short- and Long-term Variability*, The Astrophysical Journal **891** 13, URL: https://dx.doi.org/10.3847/1538-4357/ab698a (cit. on p. 4).

Cavaliere, A. G., H. Gurksy, and W. H. Tucker (1971), *Extragalactic X-ray Sources and Associations of Galaxies*, Nature **231** 437, ISSN: 1476-4687, URL: https://doi.org/10.1038/231437a0 (cit. on p. 2).

Galeazzi, M., A. Gupta, K. Covey, and E. Ursino (2006), *XMM-Newton observations of the diffuse X-ray background*, Department of Physics, University of Miami (cit. on p. 3).

Kolokythas, K. et al. (2020), *Evidence of AGN feedback and sloshing in the X-ray luminous NGC 1550 galaxy group*, Monthly Notices of the Royal Astronomical Society **496** 1471, ISSN: 1365-2966, URL: http://dx.doi.org/10.1093/mnras/staa1506 (cit. on p. 1).

Kravtsov, A. V. and S. Borgani (2012), *Formation of Galaxy Clusters*, Annual Review of Astronomy and Astrophysics **50** 353, ISSN: 0066-4146, eprint: https://www.annualreviews.org/doi/pdf/10.1146/annurev-astro-081811-125502, URL: https://www.annualreviews.org/doi/10.1146/annurev-astro-081811-125502 (cit. on p. 2).

Predehl, P. et al. (2021), *First science highlights from SRG/eROSITA: The eROSITA X-ray telescope on SRG*, A&A **647** A1 (cit. on pp. 3, 4).

Schneider, P. (2006), *Extragalactic Astronomy and Cosmology: An Introduction*, Second Edition, Springer-Verlag Berlin Heidelberg 2006, ISBN: 978-3-642-54082-0 (cit. on p. 2).

List of Figures

List of Tables